

Article

Mosaic of Anodic Alumina Inherited from Anodizing of Polycrystalline Substrate in Oxalic Acid

Sergey E. Kushnir ^{1,2,*}, Mikhail E. Kuznetsov ¹, Ilya V. Roslyakov ^{2,3}, Nikolay V. Lyskov ^{4,5}
and Kirill S. Napolskii ^{1,2}

¹ Department of Chemistry, Lomonosov Moscow State University, Moscow 119991, Russia

² Department of Materials Science, Lomonosov Moscow State University, Moscow 119991, Russia

³ Kurnakov Institute of General and Inorganic Chemistry RAS, Moscow 119991, Russia

⁴ Federal Research Center of Problems of Chemical Physics and Medical Chemistry RAS, Chernogolovka, Moscow 142432, Russia

⁵ Department of Physics, National Research University "Higher School of Economics", Moscow 101000, Russia

* Correspondence: kushnir@elch.chem.msu.ru

Abstract: The anodizing of aluminium under oscillating conditions is a versatile and reproducible method for the preparation of one-dimensional photonic crystals (PhCs). Many anodizing parameters have been optimised to improve the optical properties of anodic aluminium oxide (AAO) PhCs. However, the influence of the crystallographic orientation of an Al substrate on the characteristics of AAO PhCs has not been considered yet. Here, the effect of Al substrate crystallography on the properties of AAO PhCs is investigated. It is experimentally demonstrated that the cyclic anodizing of coarse-grained aluminium foils produces a mosaic of photonic crystals. The crystallographic orientation of Al grains affects the electrochemical oxidation rate of Al, the growth rate of AAO, and the wavelength position of the photonic band gap.

Keywords: anodizing; crystallographic orientation; photonic crystal; anodic aluminium oxide; oxalic acid



Citation: Kushnir, S.E.; Kuznetsov, M.E.; Roslyakov, I.V.; Lyskov, N.V.; Napolskii, K.S. Mosaic of Anodic Alumina Inherited from Anodizing of Polycrystalline Substrate in Oxalic Acid. *Nanomaterials* **2022**, *12*, 4406. <https://doi.org/10.3390/nano12244406>

Academic Editor: Carlos Miguel Costa

Received: 11 November 2022

Accepted: 7 December 2022

Published: 10 December 2022

Publisher's Note: MDPI stays neutral with regard to jurisdictional claims in published maps and institutional affiliations.



Copyright: © 2022 by the authors. Licensee MDPI, Basel, Switzerland. This article is an open access article distributed under the terms and conditions of the Creative Commons Attribution (CC BY) license (<https://creativecommons.org/licenses/by/4.0/>).

1. Introduction

Porous anodic aluminium oxide (AAO) films possess a unique structure with vertically aligned pores of tuneable diameter and highly controlled interpore distance in the 10–800 nm range. Such a morphology in combination with the high thermal and chemical stability of aluminium oxide makes AAO an extremely popular material for preparing membranes and templates and for other applications in modern materials science and nanotechnology [1–4].

Previously, it has been shown that the microstructure of an Al substrate influences the anodizing process. In particular, the kinetics of AAO film formation depends on the crystallographic orientation of the Al substrate. The current density is lower for stable Al facets (e.g., (111) or (100)) with dense atom packing [5]. Moreover, the degree of pore ordering is sensitive to the crystallographic orientation of the Al substrate. The smallest fraction of defects (e.g., point defects, high- and low-angle domain boundaries) has been found in AAO formed on Al(100) substrate [5–8]. The best in-plane orientational pore ordering was observed on grains with (111) orientation [5], whereas the worst ordering was found on Al(110) grains [5,8]. An inclination of the pore growth direction from the normal to the substrate governed by the crystallographic orientation of Al grains has been shown [9,10]. Furthermore, pseudo-epitaxial growth of amorphous AAO with an ordered porous structure within single-crystal grains of Al substrate was discovered [11].

As the AAO film thickness depends on the crystallographic orientation of metal grains [5,12,13], it is logical to assume that an optical path length (the product of the thickness and the effective refractive index) of the AAO should also be dependent on such

a parameter. Consequently, a lateral variation in the wavelength position of the photonic band gap (PBG) is expected if polycrystalline Al substrate is used as the starting material for anodizing. However, to the best of our knowledge, there are no reports on the influence of the Al substrate crystallography on PBG. Here, we fill this gap by studying the properties of AAO photonic crystals (PhCs) prepared by the anodizing of Al substrates with mm-sized grains of random crystallographic orientation in 0.3 M H₂C₂O₄.

2. Materials and Methods

H₂C₂O₄ × 2H₂O (99.5%), H₃PO₄ (85% aqueous solution), CrO₃ (99.7%), Br₂ (98%), and CH₃OH (99.9%) were used as received, i.e., without further purification steps. All aqueous solutions were prepared with distilled water.

To obtain Al substrates with a coarse-grained structure, high-purity Al foils (99.999%) with a thickness of 0.5 mm were annealed in air using a two-step regime: at 150 °C for 12 h and then at 500 °C for 24 h [14]. A heating rate of 5 °C min⁻¹ was used. The surfaces of the recrystallised foils were mechanically polished to a mirror finish (Figure 1a). The microstructure of the Al substrates was examined by electron backscatter diffraction (EBSD) and optical profilometry. The preparation of AAO PhCs was performed on an anodizing area of 0.986–1.250 cm² (Figure S1, Table S1) in a two-electrode electrochemical cell with an Al cathode. The 0.3 M H₂C₂O₄ electrolyte was agitated at a rate of 480 rpm using an overhead stirrer. The electrolyte was maintained at a constant temperature of 0.0 ± 0.1 °C during the anodizing. AAO PhCs were obtained by the anodizing of the Al substrates using voltage (*U*) versus charge (*Q*) modulation, *U*(*Q*) [15,16]:

$$U(Q) = U_{av} + 2.5 \sin \left(\frac{2\pi Q}{Q_0} + \frac{\pi}{2} \right), \quad (1)$$

where *U*_{av} is the average anodizing voltage, *Q*₀ = 0.53 C is the period of the *U*(*Q*) profile. The number of anodizing cycles was 100 for all the samples, and thus, the anodizing process was stopped when the total charge reached 53 C. The samples were noted as 30–35, 35–40, 40–45, 45–50, 50–55, and 55–60 for the *U*_{av} rates of 32.5, 37.5, 42.5, 47.5, 52.5, and 57.5 V, respectively. After each step of anodizing, the samples were washed repeatedly in deionised water and dried in air. After the first anodizing, the Al replicas (Figure 1c) were obtained by the selective dissolution of the AAO PhCs in a solution containing 0.5 M H₃PO₄ and 0.2 M CrO₃ at 70 °C for 30 min. Prior to the second anodizing under the same conditions as the first (Figure 1d), the topography mapping of the Al replicas was performed. To prepare free-standing 1D PhC (Figure 1e), the Al substrates were selectively dissolved in 10 vol. % bromine solution in methanol.

The grain structure of the Al substrates was examined by EBSD using a NVision 40 scanning electron microscope (Carl Zeiss AG, Oberkochen, Germany) equipped with an Nordlys IIS EBSD detector (Oxford Instruments, Abingdon, UK). EBSD maps were recorded with lateral steps of 20–50 μm.

Measurements of the topography of the Al substrates and free-standing 1D PhCs were performed using a PS50 optical profilometer (Nanovea, Irvine, CA, USA) (lateral step of 5–15 μm). To increase the reflectance of the free-standing 1D PhCs, they were covered with a 50-nm-thick Ag layer using a Q150T ES sputter coater (Quorum Technologies, Laughton, East Sussex, United Kingdom).

The spectral mapping of PhCs was performed in the transmission geometry using a setup based on an ASP-150C optical spectrometer (Avesta Project Ltd., Troitsk, Moscow, Russia). An DH-2000-DUV halogen light bulb (Ocean Optics, Largo, FL, USA) was used as a light source. The light from a 100 μm optical fibre was spatially filtered and focused on the sample (spot size of 0.1 mm, normal incidence, angular aperture of 2.5°). The transmitted light was collected by a 400 μm optical fibre and guided into the spectrum analyser. The sample was mounted on a mechanical XY translation stage to perform mapping with a step of 0.1 mm. The transmittance spectra at various incident angles were measured by rotating the sample around the axis that passed through the light beam in the sample plane.

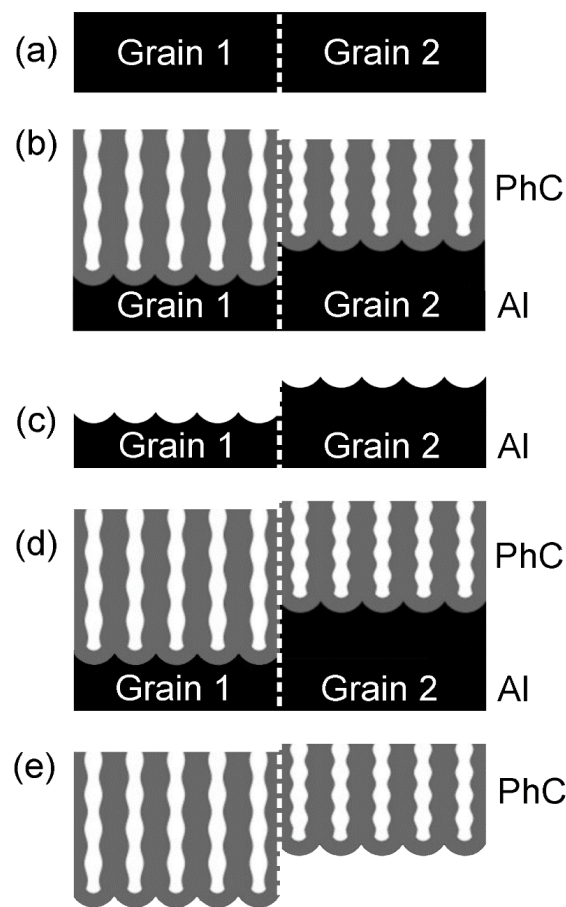


Figure 1. Synthesis of anodic aluminium oxide (AAO) one-dimensional photonic crystal (1D PhC) on coarse-grained Al. (a) Mechanically polished Al substrate; (b) 1D PhC prepared by Al anodizing; (c) Al replica after the selective dissolution of AAO PhC; (d) 1D PhC prepared by the second anodizing; (e) free-standing 1D PhC after the selective dissolution of Al.

Analysis of the Fabry–Pérot optical interference fringes was performed by fitting the positions of the extrema observed in the spectra for all measured incident angles. The fitting parameters included two Cauchy dispersion parameters, describing the dispersion of the effective refractive index of anodic oxide [17], the film thickness, and the order of interference of one of the extrema [18–20].

3. Results and Discussion

Comparing the height maps of the Al surfaces before (Figure 2a) and after (Figure 2b) the first anodizing, it can be seen that the anodizing process uncovered the grain structure of the substrate. According to the EBSD maps (Figure 2c), the anodizing area contained dozens of mm-sized grains (median size of 0.8 mm) with various crystallographic orientations. The shape of the grains on the EBSD maps is identical to the shape of the areas with the same heights, which allows one to perform a correlation analysis of the heights of the Al replica and the Al substrate crystallography. In the case of the samples obtained at anodizing voltages lower than 50 V, the dark grains in Figure 2b with a lower height correspond to the grains close to the (100) orientation (see areas with red colours on the EBSD map, Figure 2c). In contrast, the grains with higher heights (see light areas in Figure 2b) correspond to the grains close to the (111) orientation (areas with blue colours in Figure 2c). Samples 55–60 demonstrate the opposite behaviour: (111)-oriented grains possess lower height and the grains close to the (100) orientation correspond to higher areas on the Al replica (Figure 1c). As the Al was oxidised on all the metal grains simultaneously, obviously the variation in the height of the grains was caused by the variation in the Al electrochemical oxidation rate.

In other words, the rate of electrochemical oxidation of Al during anodizing depends on the crystallographic orientation of the Al substrate. For the used 0.3 M $\text{H}_2\text{C}_2\text{O}_4$ electrolyte, in the 30–50 V range, the fastest rate of electrochemical oxidation was observed for grains close to the (100) orientation, whereas (111)-oriented grains demonstrated the slowest oxidation rate. Anodizing at 55–60 V resulted in the opposite behaviour: (100)-oriented grains became more stable, whereas grains close to the (111) orientation demonstrated the fastest rate of electrochemical oxidation.

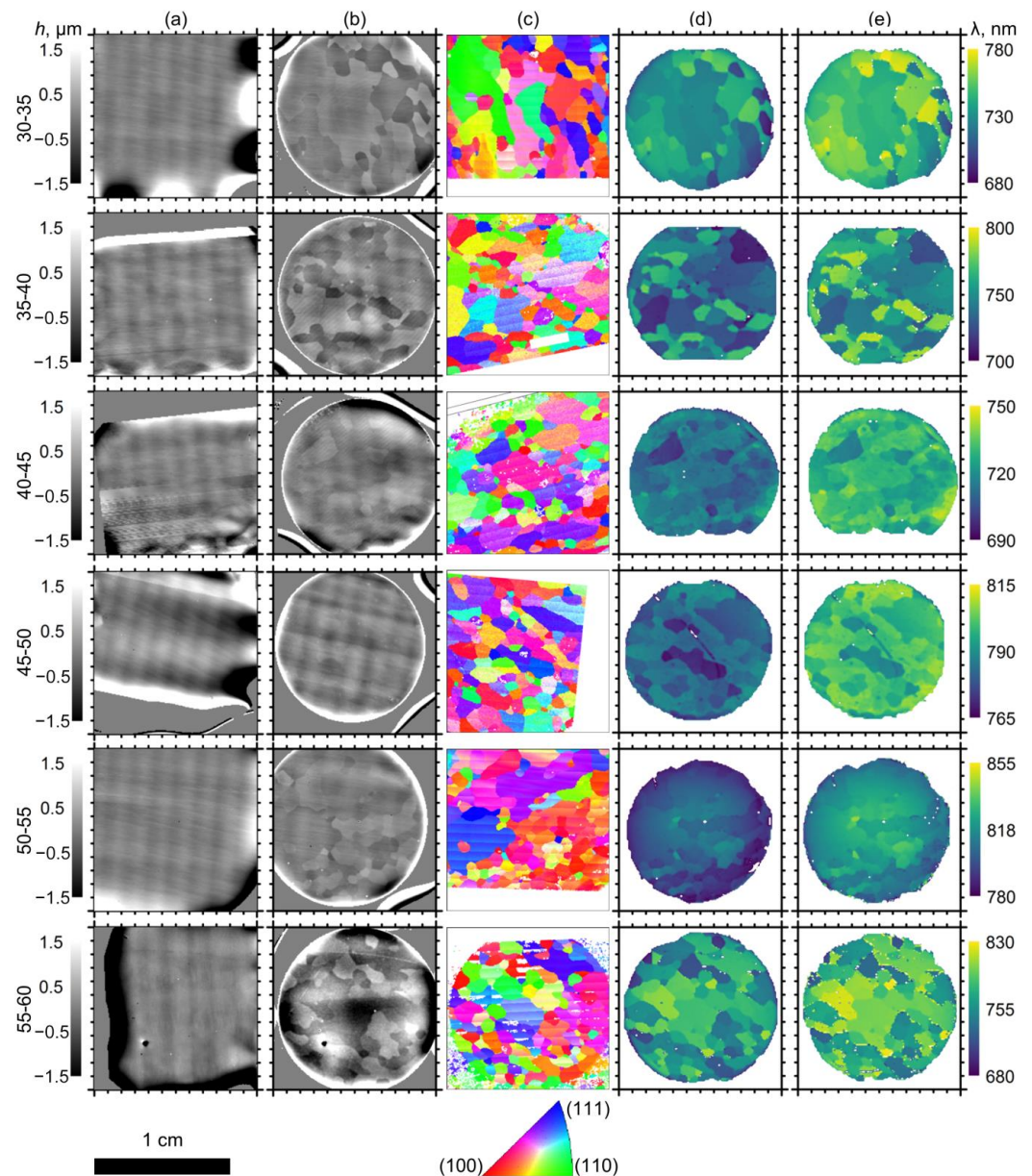


Figure 2. The mosaic of AAO PhCs obtained by anodizing of polycrystalline Al substrates. Height (h) maps of the surface of polycrystalline Al substrates before (a) and after (b) the first anodizing. (c) EBSD maps of the surface of polycrystalline Al substrates. The colours refer to the orientations shown by the inverse pole figure for the normal direction. Maps of the central wavelength (λ) of the photonic band gap (PBG) for (d) dry and (e) wet PhCs. The data in rows correspond to samples 30–35, 35–40, 40–45, 45–50, 50–55, and 55–60. All maps have a lateral size of $12 \times 12 \text{ mm}^2$. White arrows in the panels (b–d) for the sample 30–35 show the region of interest for detailed study (see Figure 3).

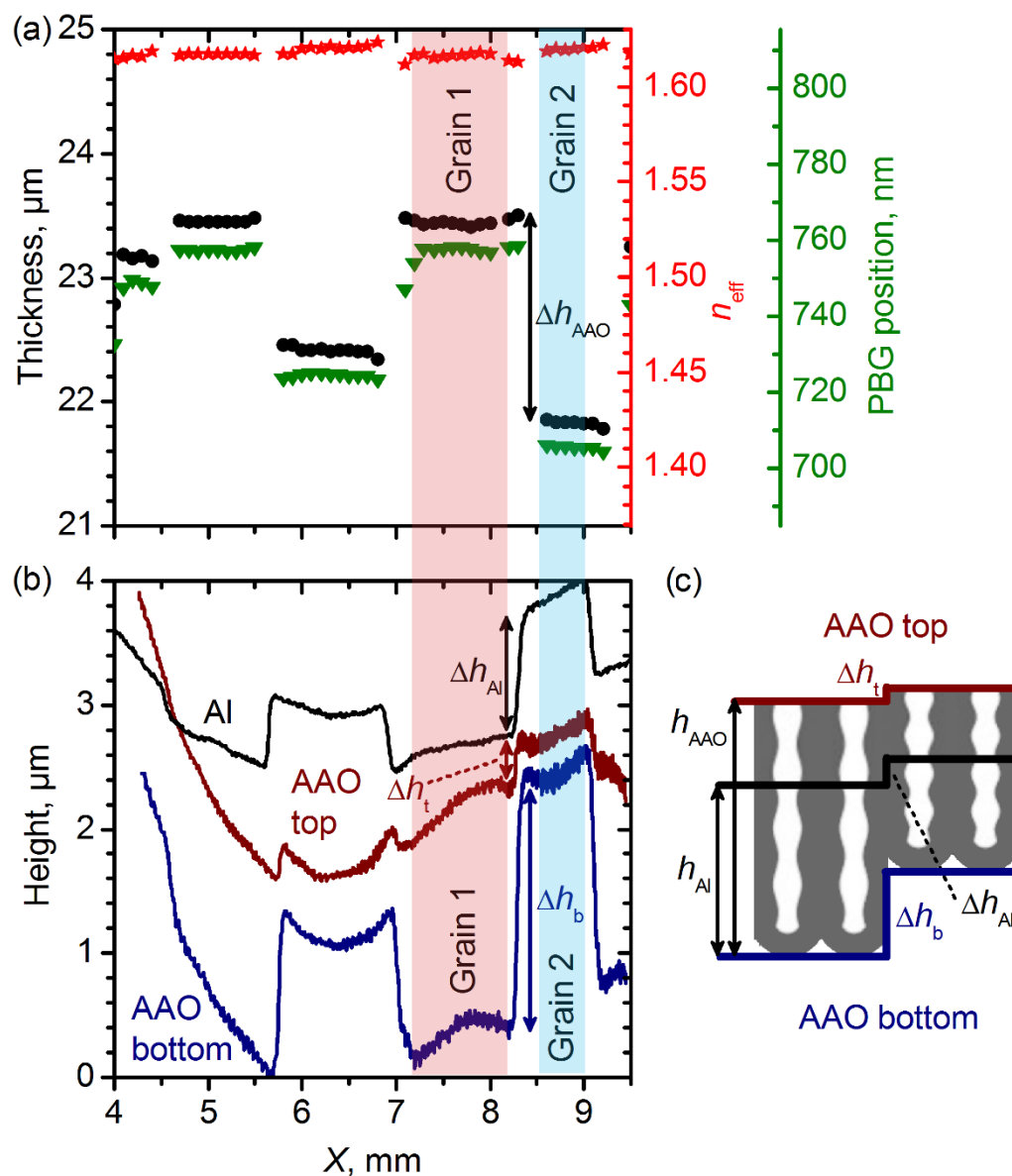


Figure 3. Analysis of profiles measured on the sample obtained at 30–35 V. (a) Profiles of thickness (black circles), the effective refractive index at 700 nm (red stars), and λ_{PBG} (green triangles). Note that the relative ranges of the vertical axes are equal to 19%. (b) Height profiles of the surface of Al substrate after the first anodizing (black) and of the top (red) and the bottom (blue) surfaces of free-standing AAO obtained after the second anodizing. (c) Scheme illustrating the places where the height profiles were measured.

The maps of the central wavelength of the PBG (λ_{PBG}), measured from the same areas as the EBSD maps, are shown in Figure 2d,e for the dry (pores filled by air) and wet (pores filled by water) samples, respectively. The λ_{PBG} values varied across the samples (Figure S2). Moreover, the grain mosaics of the spectral and EBSD maps are very similar, which clearly shows the dependence of λ_{PBG} on the Al substrate crystallography.

According to the Bragg–Snell law [21], λ_{PBG} depends on the period of the PhC structure (d), the effective refractive index of the AAO film (n_{eff}), and the angle of light incidence (θ):

$$\lambda_{\text{PBG}} = 2d\sqrt{n_{\text{eff}}^2 - \sin^2\theta}. \tag{2}$$

In the case of anodizing in self-ordering regimes at constant voltages, pore deviation from the normal orientation towards the metal surface by a small angle of 1–2 degrees was previously demonstrated [9]. The deviation value is constant within a single-crystal grain, whereas a transition through a grain boundary leads to a sudden change in the pore growth direction. On the other hand, despite various pore inclinations on different crystal grains, the AAO film grew in the normal direction. Thus, this feature of the AAO structure does not affect θ in Equation (2) and cannot describe the experimentally observed variation in the PBG position.

In the case of normal incidence, Equation (2) is simplified to:

$$\lambda_{\text{PBG}} = 2dn_{\text{eff}}. \quad (3)$$

The experimental λ_{PBG} values for the AAO PhC formed on the various Al grains varied with Al crystallography by several percentages for both the dry and wet samples. Furthermore, the wet samples showed a red shift in the λ_{PBG} compared to the dry ones. Considering Equation (3), the red shift in the λ_{PBG} for the wet samples was caused solely by the increase in the n_{eff} because the d did not change during the filling of the pores with water. According to the effective medium model [22], the n_{eff} is a function of the porosity (p), the refractive indices of the AAO cell walls (n_{cw}), and of a substance filling the pores (air or water). Thus, the ratio (r_{wd}) of the λ_{PBG} values for the wet and dry samples depends on the p and n_{cw} . According to our experiments, the r_{wd} was constant over the whole sample area and varied from 1.0196 to 1.0257 for the series of analysed AAO PhCs (Table S2). Taking into account the equality of n_{cw} for the entire sample, it can be concluded that the porosity of the AAO film did not depend on the crystallographic orientation of the Al substrate. Consequently, the n_{eff} did not depend on the crystallographic orientation of the Al substrate too and the shift in the λ_{PBG} from grain to grain was related solely to the variation in the d . As the AAO film was formed on all metal grains simultaneously, the variation in the d was caused by the variation in the AAO growth rate.

Analysis of the Fabry–Pérot optical interference fringes at different incident angles allows one to measure the n_{eff} and film thickness (h_{AAO}) [18–20,23]. Figure 3a shows the profiles of h_{AAO} , n_{eff} , and λ_{PBG} , measured along the white arrow (Figure 2, sample 30–35). The strong variation in the λ_{PBG} (green triangles) on the grain boundaries correlates with the strong variation in the h_{AAO} (black circles), whereas the n_{eff} (red stars) is almost constant. Taking account of the equal charge $Q_0 = 0.53$ C spent for the formation of each structure period and the number of anodizing cycles of 100, one can conclude that $d = h_{\text{AAO}}/100$. Thus, the shift in the λ_{PBG} was related solely to the variation in the d or the AAO growth rate.

Profilometry of the top and bottom sides of the free-standing 1D PhC was used to measure the height steps on the grain boundaries. Figure 3b shows the height profiles of the surface of the Al substrate after the first anodizing (black) and of the top (red) and bottom (blue) surfaces of the AAO. The profiles were measured along the white line indicated in Figure 2 (see data for sample 30–35). It is worth noting that the samples were not absolutely flat, but a small curvature of the sample surface (ca. 1 μm per mm) did not affect the height steps in the vicinity of grain boundaries. Differences in the electrochemical oxidation rate of Al on grains 1 and 2 caused the appearance of a step on the Al replica with a height of Δh_{Al} after the first anodizing. During the second anodizing, the charge spent for the oxidation was the same, and thus, the step height increased by a factor of 2, since the electrochemical oxidation rates remained the same. As the Al replica reproduced the bottom surface of an AAO film, the height profiles of the Al replica and the AAO bottom were identical. Indeed, the step height at the bottom of the AAO (Δh_{b}) was about $2\Delta h_{\text{Al}}$. The volume expansion during the anodizing [1] and the difference in the electrochemical oxidation rate led to a decrease in the height of the step observed on the top surface of the AAO (Δh_{t}) compared to the height difference in the Al replica after the first anodizing Δh_{Al} (Figure 3b). The difference in the thickness of the AAO (Δh_{AAO}) formed on grains 1 and 2 was $\Delta h_{\text{b}} - \Delta h_{\text{t}} = 1.65$ μm . This value is in agreement with the Δh_{AAO} obtained by the analysis of the Fabry–Pérot optical interference fringes (Figure 3a). The profilometry

and analysis of the Fabry–Pérot optical interference fringes support the above-mentioned conclusion that the shift in the λ_{PBG} from grain to grain was related solely to the variation in the structure periodicity d . According to the effective medium model [22], the equality of both the r_{wd} (Table S2) and n_{eff} (Figure 3a) for the entire sample confirms the equality of both the AAO porosity and the refractive index of the cell walls n_{CW} , i.e., their independence from the Al crystallography.

The dependence of the relative shift in the λ_{PBG} ($\Delta\lambda_{\text{PBG}}$) on the crystallographic orientation of the Al substrate is summarised in Figure 4. The dependence of $\Delta\lambda_{\text{PBG}}$ on the crystallographic orientation in the normal direction was similar to the behaviour of the rate of electrochemical oxidation of Al. In the 30–50 V range, the highest $\Delta\lambda_{\text{PBG}}$ was observed for the PhC formed on the grains close to the (100) orientation, whereas the lowest $\Delta\lambda_{\text{PBG}}$ was on the Al(111) grains. Anodizing at 55–60 V reversed the dependence: PhCs grown on the grains close to the (100) orientation showed the lowest $\Delta\lambda_{\text{PBG}}$, whereas the highest $\Delta\lambda_{\text{PBG}}$ was observed on the grains close to the (111) orientation. As $\Delta\lambda_{\text{PBG}}$ is determined mainly by the variation in the AAO PhC structure periodicity which is proportional to the AAO growth rate, then the values of $\Delta\lambda_{\text{PBG}}$ nearly equal to the values of the relative shift in the AAO growth rate.

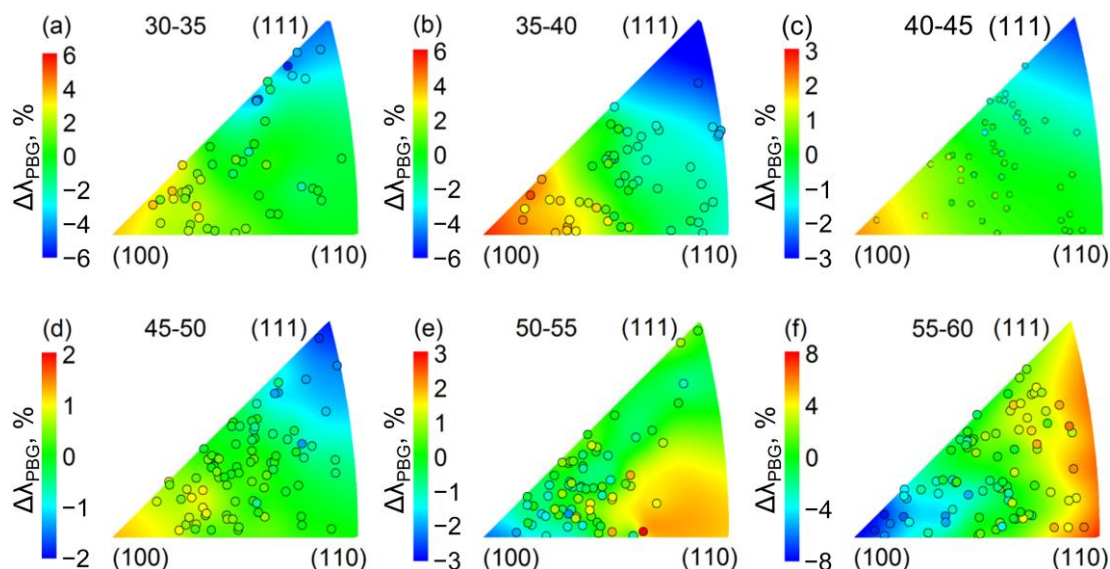


Figure 4. Dependence of the relative shift in the λ_{PBG} on the crystallographic orientation of Al substrate in the normal direction for PhCs synthesised at 30–35 V (a), 35–40 V (b), 40–45 V (c), 45–50 V (d), 50–55 V (e), 55–60 V (f). Measurements were performed in air for dry samples. Data points are shown as circles filled with the colour corresponding to the relative deviation from average λ_{PBG} and placed on the inverse pole figure in accordance with the crystallographic orientation of the Al grains. The colour map represents the smoothed experimental data for the relative shift of λ_{PBG} .

The experimental data on the dependence of the relative shift in the λ_{PBG} on the crystallographic orientation were fitted with a plane surface to determine the linear prediction of the relative shift in the λ_{PBG} for the low index surfaces of Al (Figure 5). The U_{av} in the range of 47.5–52.5 V produced more uniform AAO PhCs, whereas the U_{av} of 37.5 and 57.5 V resulted in high values of the relative PBG shift: the λ_{PBG} shifted by up to 10 and 14%, respectively, when the crystallographic orientation of the Al substrate shifted from (111) to (100). In the case of anodizing at 40 V in a 0.3 M $\text{C}_2\text{H}_2\text{O}_4$ electrolyte with and without the addition of 5% of ethanol, Al(100) has demonstrated 15% [12] and 8% [5] higher growth rates, respectively, of the AAO than Al(111). These data are in good agreement with the linear prediction of the relative shift in the λ_{PBG} .

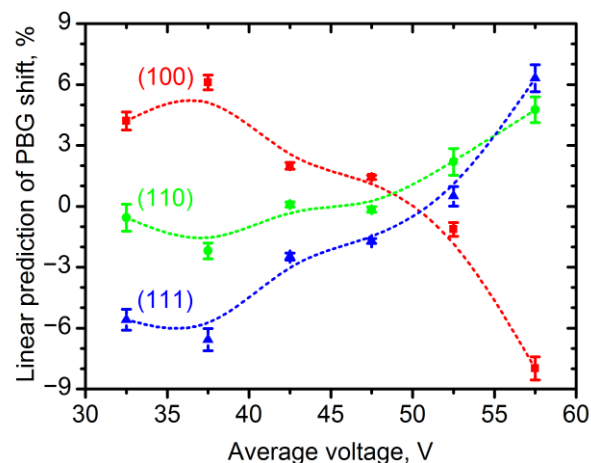


Figure 5. Linear prediction of PBG shift at low index surfaces of Al substrate versus the average voltage used for the synthesis of photonic crystals. The dashed lines are a guide for the eye.

The measured values of the shift in the λ_{PBG} are crucial for sensing the application of AAO PhCs [24–27] where the shift is an analytical response of chemical sensors. In most cases, the shift in the PBG is lower than 1% [24–27], i.e., the observed effect of the crystallographic orientation of the Al substrate on λ_{PBG} is much stronger. Thus, an analytical signal measured from different areas of an AAO PhC sensor synthesised on polycrystalline Al foil with relatively large grains of different crystallographic orientations can lead to wrong results. In photocatalysis applications, the enhancement of the photocatalytic reaction rate by the “slow photon” effect is sensitive to the distance between the edge of the PBG and the absorbance band of the organic molecules [28]. It is expected that the use of PhCs formed on polycrystalline Al substrates can result in a variation in the photocatalytic reaction rate along the sample surface, which then smooths the enhancement effect.

4. Conclusions

AAO PhCs with a grained structure were prepared by cyclic anodizing of coarse-grained Al foils in 0.3 M $\text{H}_2\text{C}_2\text{O}_4$ at 0 °C. The rate of electrochemical oxidation of Al during anodizing depends on the crystallographic orientation of the Al substrate. In the 30–50 V range, the rate of Al electrochemical oxidation increased in the order of Al(111), Al(110), Al(100), whereas the anodizing at 55–60 V reversed the order: Al(100), Al(110), Al(111). A strong correlation between the crystallographic orientation of the Al substrate in the normal direction and the central wavelength of the photonic band gap λ_{PBG} was found. The shift in the λ_{PBG} was related mainly to the variation in the AAO PhC thickness. The most uniform AAO PhCs were obtained at the average voltage of 47.5–52.5 V, whereas an average voltage of 37.5 and 57.5 V led to high values of the relative PBG shift: the λ_{PBG} shifted by up to 10 and 14%, respectively, when the crystallographic orientation of the substrate changed from Al(111) to Al(100). This effect should be considered during the synthesis of high-quality PhC structures and highly sensitive chemical sensors based on AAO. Single-crystalline or highly textured Al substrates with metal grains of similar crystallographic orientation in the normal direction are preferred for the preparation of AAO PhCs if their applications (e.g., sensing, photocatalysis, and optical filtering) require a precisely defined λ_{PBG} across the entire sample.

Supplementary Materials: The following supporting information can be downloaded at: <https://www.mdpi.com/article/10.3390/nano12244406/s1>, Figure S1: Scanned images of AAO 1D PhCs.; Table S1: Anodizing area (cm^2) of prepared anodic aluminium oxide one-dimensional photonic crystals; Table S2: The ratio (r_{wd}) of the λ_{PBG} values for wet and dry samples over the entire sample area of prepared anodic aluminium oxide one-dimensional photonic crystals; Figure S2: Transmittance spectra of sample 30–35 measured in the spots grown on grains close to Al(100) and Al(111).

Author Contributions: Conceptualisation, S.E.K.; methodology, S.E.K.; software, S.E.K.; validation, S.E.K. and M.E.K.; formal analysis, S.E.K. and M.E.K.; investigation, S.E.K., I.V.R. and N.V.L.; resources, I.V.R., N.V.L. and K.S.N.; data curation, S.E.K.; writing—original draft preparation, S.E.K.; writing—review and editing, S.E.K., M.E.K., I.V.R. and K.S.N.; visualisation, S.E.K. and M.E.K.; supervision, S.E.K.; project administration, S.E.K.; funding acquisition, S.E.K. All authors have read and agreed to the published version of the manuscript.

Funding: This research was funded by the Russian Science Foundation, grant No. 22-23-00973 (<https://rscf.ru/project/22-23-00973/> (accessed on 1 November 2022)).

Data Availability Statement: The data presented in this study are available in the article.

Acknowledgments: The Interdisciplinary Scientific and Educational School of Moscow University «Future Planet: Global Environmental Change» is acknowledged. Some parts of the experiments were carried out using the scientific equipment purchased by the M.V. Lomonosov Moscow State University Program of Development. The EBSD technique was carried out at the Joint Research Centre for Physical Methods of Research located at the Kurnakov Institute of General and Inorganic Chemistry RAS. FRC PCP and MC RAS (state task No. AAAA-A19-119061890019-5) are acknowledged for the opportunity to use the Nanovea PS50 optical profilometer.

Conflicts of Interest: The authors declare no conflict of interest.

References

1. Lee, W.; Park, S.-J. Porous Anodic Aluminum Oxide: Anodization and Templated Synthesis of Functional Nanostructures. *Chem. Rev.* **2014**, *114*, 7487–7556. [[CrossRef](#)] [[PubMed](#)]
2. Wen, L.; Wang, Z.; Mi, Y.; Xu, R.; Yu, S.-H.; Lei, Y. Designing Heterogeneous 1D Nanostructure Arrays Based on AAO Templates for Energy Applications. *Small* **2015**, *11*, 3408–3428. [[CrossRef](#)] [[PubMed](#)]
3. Md Jani, A.M.; Losic, D.; Voelcker, N.H. Nanoporous Anodic Aluminium Oxide: Advances in Surface Engineering and Emerging Applications. *Prog. Mater. Sci.* **2013**, *58*, 636–704. [[CrossRef](#)]
4. Sulka, G.D.; Brzózka, A.; Zaraska, L.; Wierzbička, E.; Brudzisz, A. AAO Templates with Different Patterns and Channel Shapes. In *Submicron Porous Materials*; Springer: Cham, Switzerland, 2017; pp. 107–156. ISBN 978-3-319-53033-8.
5. Roslyakov, I.V.; Koshkodaev, D.S.; Eliseev, A.A.; Hermida-Merino, D.; Ivanov, V.K.; Petukhov, A.V.; Napol'skii, K.S. Growth of Porous Anodic Alumina on Low-Index Surfaces of Al Single Crystals. *J. Phys. Chem. C* **2017**, *121*, 27511–27520. [[CrossRef](#)]
6. Beck, G.; Bretzler, R. Regularity of Nanopores in Anodic Alumina Formed on Orientated Aluminium Single-Crystals. *Mater. Chem. Phys.* **2011**, *128*, 383–387. [[CrossRef](#)]
7. Ng, C.K.Y.; Ngan, A.H.W. Precise Control of Nanohoneycomb Ordering over Anodic Aluminum Oxide of Square Centimeter Areas. *Chem. Mater.* **2011**, *23*, 5264–5268. [[CrossRef](#)]
8. Sacco, L.; Florea, I.; Châtelet, M.; Cojocaru, C.-S. Investigation of Porous Anodic Alumina Templates Formed by Anodization of Single-Crystal Aluminum Substrates. *Thin Solid Films* **2018**, *660*, 213–220. [[CrossRef](#)]
9. Roslyakov, I.V.; Eliseev, A.A.; Yakovenko, E.V.; Zabelin, A.V.; Napol'skii, K.S. Longitudinal Pore Alignment in Anodic Alumina Films Grown on Polycrystalline Metal Substrates. *J. Appl. Crystallogr.* **2013**, *46*, 1705–1710. [[CrossRef](#)]
10. Roslyakov, I.V.; Koshkodaev, D.S.; Eliseev, A.A.; Hermida-Merino, D.; Petukhov, A.V.; Napol'skii, K.S. Crystallography-Induced Correlations in Pore Ordering of Anodic Alumina Films. *J. Phys. Chem. C* **2016**, *120*, 19698–19704. [[CrossRef](#)]
11. Napol'skii, K.S.; Roslyakov, I.V.; Romanchuk, A.Y.; Kapitanova, O.O.; Mankevich, A.S.; Lebedev, V.A.; Eliseev, A.A. Origin of Long-Range Orientational Pore Ordering in Anodic Films on Aluminium. *J. Mater. Chem.* **2012**, *22*, 11922–11926. [[CrossRef](#)]
12. Evertsson, J.; Vinogradov, N.A.; Harlow, G.S.; Carlà, F.; McKibbin, S.R.; Rullik, L.; Linpé, W.; Felici, R.; Lundgren, E. Self-Organization of Porous Anodic Alumina Films Studied in Situ by Grazing-Incidence Transmission Small-Angle X-ray Scattering. *RSC Adv.* **2018**, *8*, 18980–18991. [[CrossRef](#)] [[PubMed](#)]
13. Vinogradov, N.A.; Harlow, G.S.; Carlà, F.; Evertsson, J.; Rullik, L.; Linpé, W.; Felici, R.; Lundgren, E. Observation of Pore Growth and Self-Organization in Anodic Alumina by Time-Resolved X-ray Scattering. *ACS Appl. Nano Mater.* **2018**, *1*, 1265–1271. [[CrossRef](#)]
14. Gordeeva, E.O.; Roslyakov, I.V.; Napol'skii, K.S. Aluminium Anodizing in Selenic Acid: Electrochemical Behaviour, Porous Structure, and Ordering Regimes. *Electrochim. Acta* **2019**, *307*, 13–19. [[CrossRef](#)]
15. Sapoletova, N.A.; Kushnir, S.E.; Napol'skii, K.S. Anodic Titanium Oxide Photonic Crystals Prepared by Novel Cyclic Anodizing with Voltage versus Charge Modulation. *Electrochem. Commun.* **2018**, *91*, 5–9. [[CrossRef](#)]
16. Kushnir, S.E.; Sapoletova, N.A.; Roslyakov, I.V.; Napol'skii, K.S. One-Dimensional Photonic Crystals with Nonbranched Pores Prepared via Phosphorous Acid Anodizing of Aluminium. *Nanomaterials* **2022**, *12*, 1548. [[CrossRef](#)] [[PubMed](#)]
17. Ermolaev, G.A.; Kushnir, S.E.; Sapoletova, N.A.; Napol'skii, K.S. Titania Photonic Crystals with Precise Photonic Band Gap Position via Anodizing with Voltage versus Optical Path Length Modulation. *Nanomaterials* **2019**, *9*, 651. [[CrossRef](#)] [[PubMed](#)]

18. Kushnir, S.E.; Napolskii, K.S. Thickness-Dependent Iridescence of One-Dimensional Photonic Crystals Based on Anodic Alumina. *Mater. Des.* **2018**, *144*, 140–150. [[CrossRef](#)]
19. Sapoletova, N.A.; Kushnir, S.E.; Cherepanova, Y.M.; Napolskii, K.S. Effect of Heat Treatment on the Structure and Optical Properties of Porous Anodic Titanium Oxide Films. *Inorg. Mater.* **2022**, *58*, 40–47. [[CrossRef](#)]
20. Sapoletova, N.A.; Kushnir, S.E.; Napolskii, K.S. Polarization-Enhanced Cell Walls Etching of Anodic Titanium Oxide. *Nanotechnology* **2022**, *33*, 065602. [[CrossRef](#)]
21. Ozin, G.A.; Arsenault, A. *Nanochemistry: A Chemical Approach to Nanomaterials*; Royal Society of Chemistry: London, UK, 2015; ISBN 978-1-78262-626-8.
22. Choy, T.C. *Effective Medium Theory: Principles and Applications*, 2nd ed.; Oxford University Press: Oxford, UK, 2016; ISBN 978-0-19-870509-3.
23. Kushnir, S.E.; Pchelyakova, T.Y.; Napolskii, K.S. Anodizing with Voltage versus Optical Path Length Modulation: A New Tool for the Preparation of Photonic Structures. *J. Mater. Chem. C* **2018**, *6*, 12192–12199. [[CrossRef](#)]
24. Acosta, L.K.; Bertó-Roselló, F.; Xifre-Perez, E.; Santos, A.; Ferré-Borrull, J.; Marsal, L.F. Stacked Nanoporous Anodic Alumina Gradient-Index Filters with Tunable Multi-Spectral Photonic Stopbands as Sensing Platforms. *ACS Appl. Mater. Interfaces* **2019**, *11*, 3360–3371. [[CrossRef](#)] [[PubMed](#)]
25. Law, C.S.; Lim, S.Y.; Abell, A.D.; Voelcker, N.H.; Santos, A. Nanoporous Anodic Alumina Photonic Crystals for Optical Chemo- and Biosensing: Fundamentals, Advances, and Perspectives. *Nanomaterials* **2018**, *8*, 788. [[CrossRef](#)] [[PubMed](#)]
26. Kumeria, T.; Rahman, M.M.; Santos, A.; Ferré-Borrull, J.; Marsal, L.F.; Losic, D. Structural and Optical Nanoengineering of Nanoporous Anodic Alumina Rugate Filters for Real-Time and Label-Free Biosensing Applications. *Anal. Chem.* **2014**, *86*, 1837–1844. [[CrossRef](#)] [[PubMed](#)]
27. Kumeria, T.; Rahman, M.M.; Santos, A.; Ferré-Borrull, J.; Marsal, L.F.; Losic, D. Nanoporous Anodic Alumina Rugate Filters for Sensing of Ionic Mercury: Toward Environmental Point-of-Analysis Systems. *ACS Appl. Mater. Interfaces* **2014**, *6*, 12971–12978. [[CrossRef](#)] [[PubMed](#)]
28. Lim, S.Y.; Law, C.S.; Markovic, M.; Marsal, L.F.; Voelcker, N.H.; Abell, A.D.; Santos, A. Rational Management of Photons for Enhanced Photocatalysis in Structurally-Colored Nanoporous Anodic Alumina Photonic Crystals. *ACS Appl. Energy Mater.* **2019**, *2*, 1169–1184. [[CrossRef](#)]